IOPscience iopscience.iop.org

Home Search Collections Journals About Contact us My IOPscience

Dynamical regimes of a granular gas in microgravity : a molecular dynamics study

This article has been downloaded from IOPscience. Please scroll down to see the full text article.

2011 J. Phys.: Conf. Ser. 327 012035

(http://iopscience.iop.org/1742-6596/327/1/012035)

View the table of contents for this issue, or go to the journal homepage for more

Download details:
IP Address: 139.165.105.154
The article was downloaded on 27/01/2012 at 08:34

Please note that terms and conditions apply.

Journal of Physics: Conference Series **327** (2011) 012035 doi:10.1088/1742-6596/327/1/012035

Dynamical Regimes of a Granular Gas in Microgravity : a Molecular Dynamics Study

E. Opsomer, F. Ludewig and N. Vandewalle

GRASP Université de Liège, Allée du 6 Aôut, B-4000 Liège

E-mail: eric.oposmer@doct.ulg.ac.be

Abstract. We propose a numerical model, based on molecular dynamics, which is able to reproduce the behavior of a dissipative granular gas in microgravity. Granular material is confined in a cubic box of side length L following a sinusoidal motion of amplitude A and angular velocity $\omega = 2\pi f$ along the z-axis. The simulations are performed using the parameters of earlier Texus experiments [15]. Our results are in excellent agreement with experimental data. Moreover, we discovered various dynamical regimes and the physical conditions for their appearance : a gaseous state, the formation of either small or large clusters, the collective motion of grains. Phase diagrams are drawn where transitions between these different granular states are emphasized. Transitions are discussed by considering Statistical Physics models.

1. Introduction

The intriguing behaviors of grains and powders fascinate scientists since the nineteenth century. Properties like Reynolds dilatancy [1], Brazil Nut effect [2, 3], heterogenous force networks [4, 5] and clustering [6, 15] have been discovered. Nowadays, granular material like coal, sand and even powders are part of all economic activity such as agriculture, construction, cosmetics and aerospace research.

Different granular states could be encountered. Solid and liquid states have been deeply investigated during the last decades by studying granular compaction [7, 8, 9] and granular flows [10, 11]. A great number of models were suggested but could not give complete answers to all fundamental questions [12]. Among all phases, gaseous are the most complex. The dissipative character of the collisions implies a constant external energy supply and microgravity to subsist. Indeed, experimentation with granular material requires parabolic flights, sounding rockets, drop tower experiments or ISS missions that are bound to high costs and long preparation times. Nevertheless, these micro-gravity studies are of an capital interest in order to prepare longtime space missions, to study the impact of asteroids [13] or to understand the dynamics of planetary rings [14].

Pioneer work has been done by Falcon *et al.* during Mini-Texus 5 experimentation [15, 16]. Clustering has been reported and refers to particles mostly remaining in the center of the box, forming a denser region in the system. Incoming particles are trapped in the cluster, while other particles leave the dense region. Different mechanisms like inelastic collapse [17] have been proposed to explain the clustering phenomenon. A criterion for the appearance of the cluster has been proposed, based on experimental observation. It is related to the number of grain layers inside the box. Low densitiy granular gases have been investigated by Evesque [18].

Published under licence by IOP Publishing Ltd

Local measures of granular pressure and granular temperature as well as exponential velocity distributions were reported. Numerical simulations have been realized and sustain experimental results.

However, the behavior of granular gases, especially for extreme densities, is still not well understood. Given the great number of parameters, too few experiments have been realized and nowadays no model is able to describe completely the behavior of this material. A lot of fundamental research will be needed to illuminate the remaining questions.

2. Model

In opposition to classical Event Driven algorithm (ED) [17, 19] for which inelastic collapse is avoided by a time cutoff model [20], we are using a three-dimensional model based on Molecular Dynamics (MD) [21, 22]. A cubic container of side length L, following a sinusoidal motion of amplitude A and angular velocity $\omega = 2\pi f$ along the z-axis, is filled with N spherical particles of mass m and a radius r. At initialization, each one is given a different random position (that allows no contact between the particle and the rest of the system). Moreover, their initial linear and angular velocities are null. Contact forces are computed following two simple models.

Normal forces F_{ij}^n are composed by a repulsive (F_{ij}^{rep}) and a dissipative (F_{ij}^{dis}) component. The repulsive component follows a simple Hooke's Law

$$F_{ij}^{rep} = -k_n \delta_{ij} \tag{1}$$

where $\delta_{ij} = d_{ij} - 2r$ with d_{ij} the distance between the centers of the solids i and j. The constant k_n is the normal stiffness which is a purely numerical parameter. Indeed, this stiffness is not linked to specific physical properties of the simulated material. It's value is calculated in order to keep the static deformation of the particles lower than $10^{-4}r$. (In our simulations k_n ranges typically between 100 and 1000 kg/s^2). The dissipative component is taken into account by viscous forces according to the following law

$$F_{ij}^{dis} = -\gamma_n(k_n, \varepsilon)\frac{\partial \delta_{ij}}{\partial t} \tag{2}$$

where the viscous constant γ_n is a non-trivial function of the normal stiffness k_n and the restitution coefficient ε. This restitution coefficient is used for both, grain-grain and grain-wall collisions. In opposite to other models (like Hertz' model) using a Hooke's Law and viscous dissipation allows us to work with a constant contact duration Δt, independent on the impact velocities. In order to assure the integration of the forces, each contact should be resolved in about 100 time steps τ (*i.e.* $\tau \approx \Delta t/100$).

Tangent forces F_{ij}^t are bounded and depend on the relative tangent velocities v_{ij}^t between the colliding solids i and j. One has

$$F_{ij}^t = -k_t v_{ij}^t \quad \text{and} \quad \|F_{ij}^t\| \leq \mu F_{ij}^n \tag{3}$$

where μ is a friction coefficient and k_t a purely numerical constant. Friction coefficient μ as wall as restitution coefficient ε can be adapted to fit the intrinsic properties of the system. A complete description of MD simulations is given by Taberlet [23].

3. Results

In our simulations, we reproduced the results of Falcon *et al* [15]. Three cubic cells of side length $L = 10$ mm are filled with bronze spheres of radius $r = 0.175$ mm. The system is oscillating with an amplitude $A = 2.5$ mm and a frequency $f = 30$ Hz. According to the materials properties, friction coefficient is set to $\mu = 0.2$, restitution coefficient to $\varepsilon = 0.9$ and volume density to $\rho = 8\ 10^3$ kg/m^3. Figure 1 presents simulations and experiments of the system with $N = 1420$, 2840 and 4510 particles at its maximum downward velocity $-A\omega$. Dense regions are observed thanks to shading effects [15].

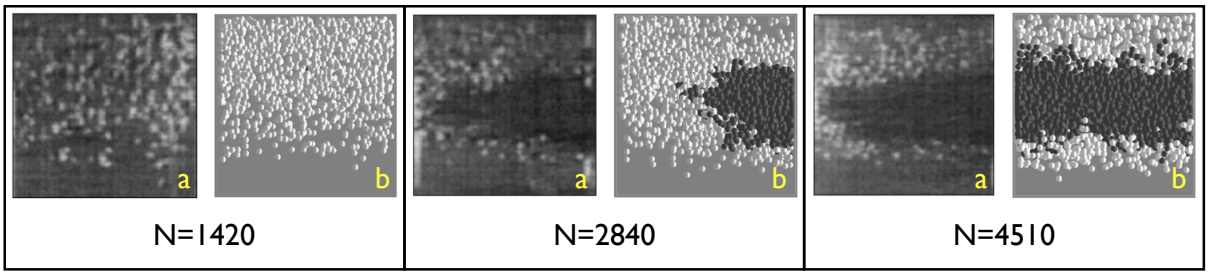

Figure 1. (a) The experimental results for respectively N=1420, 2840 and 4510 particles at the box maximum downward velocity [15]. (b) Numerical results in the same conditions. Shading of the cluster is realized by a proximity rule described in the text.

The right three pictures (b) correspond to our simulations where dense regions are blackened according to a simple proximity rule : (i) Two particles are neighbors if the distance between them is less than $2.5r$. (ii) Particles that are close enough to the system's center of mass are forming a seed. (iii) Step by step, the seed is extended by its neighbors. (iv) At saturation, the cluster is colored in black (see Figure 1). Simulations are in a qualitative agreement to Falcon's experiment presented in pictures (a). Indeed, the less dense system ($N = 1420$) of Figure 1 stays in a gaseous state and presents a density gradient decreasing towards the center of the box. For the densest case ($N = 4510$) clustering is observed around the center of the box. Moreover, the distribution is homogeneous over the xy-plane. Finally, the intermediate case ($N = 2840$) presents a new phenomenon : the cluster does not occupy the entire xy-plane. That behavior was not addressed in Falcon's experiment but can be seen on their pictures.

After the reproduction of the Texus experiments and the detection of partial clustering, the second step was to modify the different parameters. We decided to investigate the behavior of a system with a large number of grains. At this point, the densest system ($N = 4510$) had only a global density of $\eta = 0.11$. By progressively increasing the number of grains up to $N = 6800$ ($\eta \approx 0.15$) a fourth state has been found. Particles stay gathered and present a coherent motion with a velocity close to $\pm A\omega$. Figure 2 describes the different dynamical regimes of a system with respectively $N = 1420, 2840, 4510$ and 6800 grains at its maximum downwards velocity $-A\omega$. Different colors correspond to selected ranges of the vertical velocity : blue if $|v_z| < A\omega$, green if $A\omega \leq |v_z| < 2A\omega$ and orange if $2A\omega \leq |v_z|$.

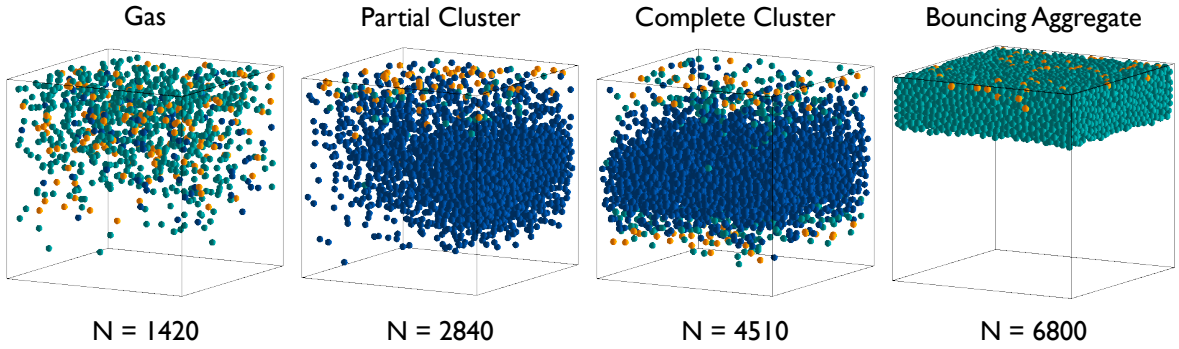

Figure 2. By increasing the grain number N, one can observe four different dynamical regimes: a gaseous phase, partial and complete clustering and an aggregate phase. Color stand for different velocity ranges: Blue for subsonic grains, green for velocities between one and two times the maximum velocity of the box and orange for even higher velocities.

Each dynamical regime is discussed in the following and introduced by two figures. On the left, the Probability Density Function (PDF) of particle positions, along the three axis, collected at the systems maximum velocities $\pm A\omega$. On the right, the PDF of U, the vertical velocities of the particles normalized by $A\omega$. Data is collected at the systems maximum downward velocity $-A\omega$.

3.1. Gas state

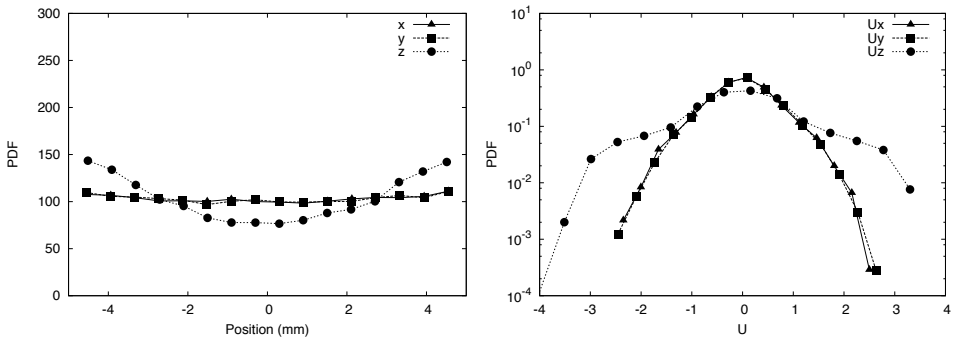

Figure 3. (Left) PDF of particle positions in the system collected every half period. (Right) Semi-log PDF plot of particle velocities in the gaseous state.

The gaseous state is found in dilute systems, the grains exhibit a broad and asymmetric distribution of vertical velocities v_z as shown in Figure 3. This asymmetry evolves according to the phase oscillation of the box. Particles can be found everywhere in the system, but follow a density gradient decreasing from one wall towards the center of the box, as shown in Figure 2 and 3. According to earlier experimentations [24, 25], we found v_x and v_y distributions of the form $P_\lambda^\gamma(v) = \lambda \exp(-|\lambda v|^\gamma), \gamma \in \{1, 2\}$ and λ as fitting parameter. Note that $\lambda \approx \frac{1}{v_0}$, where v_0 is the mean velocity. A γ value is preferred to another depending on the velocity range in the system.

3.2. Partial Cluster

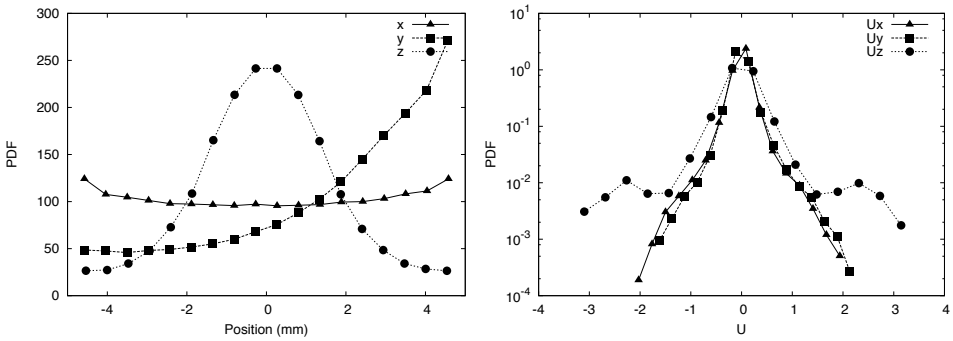

Figure 4. (Left) PDF of particle positions in the system collected every half period. (Right) Semi-log PDF plot of particle velocities in the a partial cluster.

When the number of grains increases, the system could present a partial clustering. Particles are more or less stabilized around the origin of the z-axis but stay gathered along a wall of the box. One could assumed that the system needs a typical cluster width to be energetically stable. In the distribution of velocities along z (Figure 4), a sharp peak appears around zero which is a signature for clustering. However, the distribution exhibits a broad foot since a gaseous regime coexists in the system. Multiple simulations have shown that a cluster can appear on a particular lateral wall with a probability 1/4. Moreover, simulations in a cylinder with identical volume and base section revealed that the lateral clustering is not related to corner effects. The reason of this phenomenon is yet not well understood

3.3. Complete Cluster

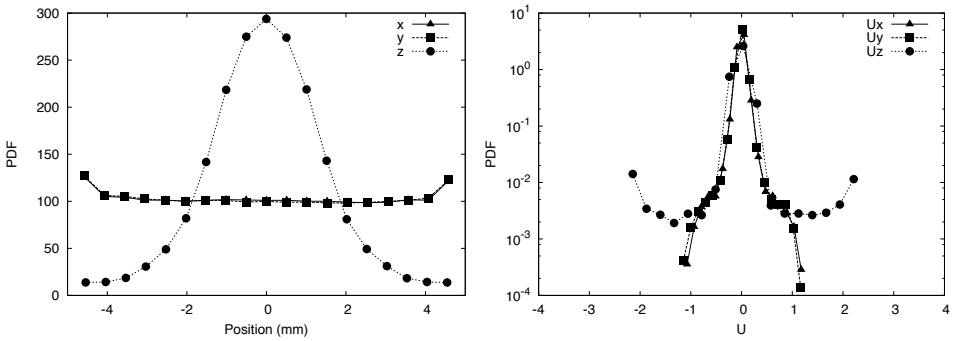

Figure 5. (Left) PDF of particle positions in the system collected every half period. (Right) Semi-log PDF plot of particle velocities in the a complete cluster.

When the density further increases, we observe that the cluster spreads over the entire xy plane. A peaked velocity distribution around zero can be observed in Figure 5. The presence of two sharp peaks at $v_z = \pm 2A\omega$ (also seen for partial clustering) is due to the granular gas trapped in between the cluster and the vibrating walls. We assist to an equilibrium between condensation and evaporation of the cluster. By tracking particles and analyzing the dynamics of clusterisation during several periods, we can conclude that the cluster is in a dynamical state with a constant renewal. Indeed, high speed particles arriving from the walls crush into the cluster, dissipate their energy and eventually become part of the cluster. The energy partially

transmitted across the cluster provokes internal rearrangements and eventually ejects particles. It should be noted that the packing fraction measured inside the cluster is about $\eta = 0.30$ which is far below the jamming limit.

3.4. Bouncing aggregate

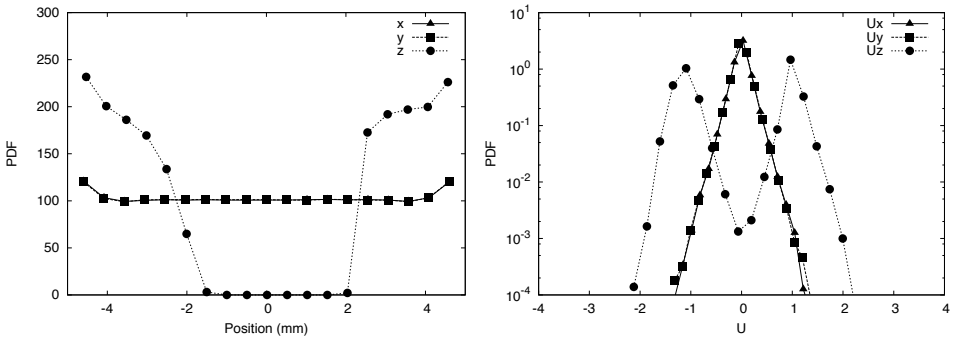

Figure 6. (Left) PDF of particle positions in the system collected every half period. (Right) Semi-log PDF plot of particle velocities in a bouncing aggregate.

For denser systems a new phenomenon is observed. The important amount of granular material confined in the system leads to higher kinetic energy than in other regimes (see figure 9). This energy cannot only be dissipated through successive collisions like in a cluster. Indeed, the local density in the system's center is high enough to assure permanent contacts between many particles, when the gaseous phase encounters this denser region all the grains a dragged towards the wall. This bouncing state is characterized by a coherent motion of all particles and peaked velocity distribution around $\pm A\omega$. Particles stay gathered in a dense arrangement which describes a movement similar to a totally dissipative bouncing ball [26]. Moreover, density distribution along the z-axis revealed crystal-like structures inside the packing. Layers are observed along the three axes.

4. Discussion

4.1. Phase Diagrams

An automated and reliable detection of the different dynamical regimes can be done by statistical means. The complete cluster detection relies a two-sample Kolmogorov-Smirnov (KS) test [27] with a significance level $\alpha = 0.01$. The KS test compares the cumulative distribution function (CDF) of a uniform distribution with the CDF of the particles distribution along z axis. The null hypothesis (H_0) of the test is the assumption that the observed distribution is uniform, hence that the system is gaseous. The alternative hypothesis is noted (H_1). We define the parameter D as the following

$$D = \sup_{|z| \leq L/2} \|F(z) - U(z)\| \tag{4}$$

where $F(z)$ is the observed CDF of the particles distribution along z-axis and $U(z)$ the theoretical uniform distribution. The KS test value is defined by $T_z = D\sqrt{n/2}$ where n is the number of classes. H_0 is rejected at level α if $T_z > K_\alpha$. The statistical threshold K_α can be found in tables. In a partial cluster regime, the system displays a strong heterogeneity in the xy-plane, therefore its detection relies on a two-sample KS test between the particles distribution along the x and y-axes with a significance level $\alpha = 0.01$. The test is denoted by T_{xy}. Finally, bouncing regime is detected by analyzing frequency fluctuations in the center of the box. If the central part of the

box has a density at least two times lower than the one corresponding to a uniform distribution, the system is evolving like an inelastic body bouncing between two oscillating plates. A large number of MD simulations allowed us to obtain four typical (η, r) phase diagrams that are shown in figure 7.

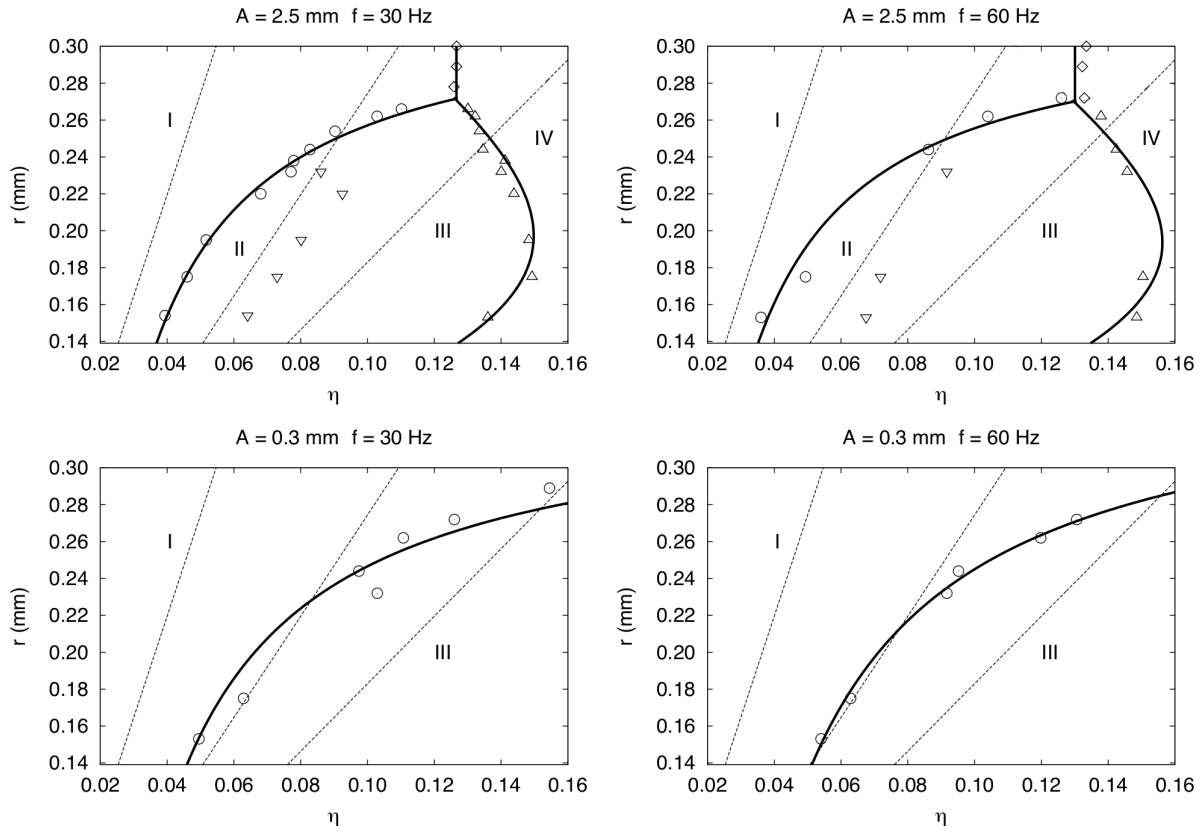

Figure 7. Simulated (r,η) phase diagrams for two different amplitudes $A = 2.5$ mm and $A = 0.3$ mm and for two different frequencies $f = 30$ Hz and $f = 60$ Hz. Curves correspond to the transitions from one dynamical regime to another. Differnt phases are denoted by numbers from I to IV.

For high amplitude ($A = 2.5$ mm), the four dynamical regimes can be observed and are denoted on figure 7 (I gas, II partial cluster, III complete cluster and IV aggregate). For low amplitude ($A = 0.3$ mm), only the gas and the complete cluster state is observed. Parameters such as η, r and A seem to have a deep impact on the systems dynamics in opposite to ω whose fluctuations have only minor effects. The emergence of a cluster for low amplitude is not trivial. While the formation of a high density zone in the case of $A = L/4 = 2.5$ mm could be triggered by geometrical reasons and confinement, the appearance of such a dynamical regime for $A = 0.3$ mm requires the presence of additional phenomena such as inelastic collapse. Moreover, measuring the standard deviation σ of the position PDF along the z-axis for 2 simulations with $N = 5000$, $r = 0.175$ mm and respectively $A = 2.5$ mm and $A = 0.3$ mm shows us that the difference of the cluster width is negligible compared to the difference of amplitude. Collecting data every period, we found in the first case $\sigma_{2.5} = 1.51$ mm and in the second $\sigma_{0.3} = 1.72$ mm. Figure 8 shows the position PDF along z-axis for both simulations. Shaded zones refer to the volume visited by the box' walls during oscillation.

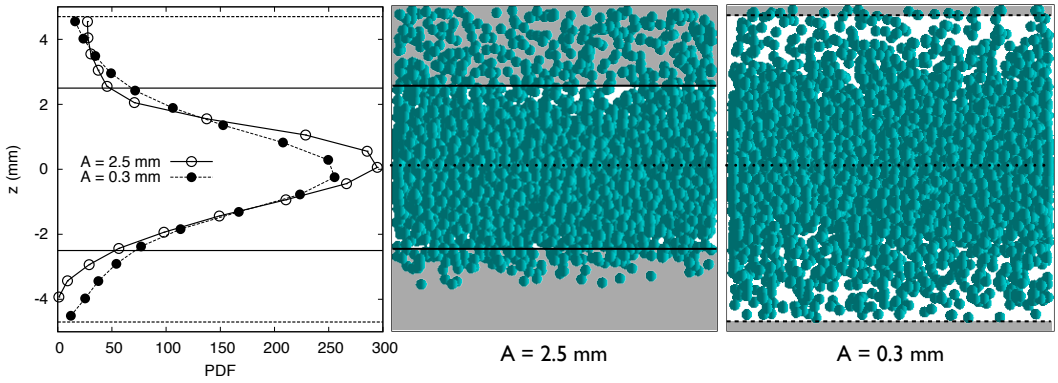

Figure 8. (Left) Distribution of the particle positions along z-axis for 2 simulations with $N = 5000$, $r = 0.175$ mm and respectively $A = 2.5$ mm and $A = 0.3$ mm. Data is collected every period. (Center) Lateral view of the system with an amplitude of $A = 2.5$ mm. (Right) Lateral view of the system with an amplitude of $A = 0.3$ mm. Shaded zones refer to the volume visited by the box' walls during oscillation.

4.2. Transition lines

For large amplitudes, the (r, η)-phase diagrams, illustrated in the first row of Figure 7, exhibit all the dynamical regimes. Different regimes are separated by transition curves that meet on triple points. Earlier studies [15] considered that cluster may be expected once there is initially more than a single layer of particles in the system. In this configuration, particle-particle collisions become frequent events which encourages dissipation and thus cluster formation. In our phase diagram, iso-layer curves correspond to dashed straight lines with an angular coefficient proportional to the inverse number of granular layers. The layer criterion clearly misses the transition from a gas to a (partial) cluster. The (◯)frontier is better described by the empirical law

$$r_{clust} - r = \delta_{clust} \left(\frac{1 - \eta}{\eta} \right) \tag{5}$$

where δ_{clust} and r_{clust} are constants. Eq. (5) supports two arguments : (i) a critical size $r_{clust} \approx 0.32$ mm for the grains above which no cluster appears, and (ii) the ratio between free volume and occupied volume becomes a relevant parameter. It should be noted that this ratio is also relevant for describing mean free path in our system.

The transition between partial and complete clustering is rather complex. One should note that partial clustering is only present for small particles and large amplitudes and. Moreover, it needs a long formation time (about 100 periods).

The bouncing aggregate regime IV appears for large packing fractions. Large particles condensate without clustering. The ◊-frontier between gaseous and condensed states is a vertical line of equation $\eta = 0.127$. Considering the whole granular assembly as a single inelastic body, this critical value can be established theoretically by adapting latest results concerning the Fermi-Box problem [28]. A punctual body is confined in a box of height H which follows a sinusoidal motion of amplitude A. For a restitution coefficient $\varepsilon = 0$, it is shown that the dynamics switch from a mono-periodical motion (similar to the diluted gaseous state) to a regime presenting sticking phenomena (similar to the condensed state) once the critical height $h = (H/A) = \pi$

is reached. In our case, the size of the particles cannot be neglected, therefore the Fermi-Box condition becomes

$$\frac{L - \left(\frac{L\eta^*}{\eta_{rlp}}\right)}{A} = \pi \tag{6}$$

where the random loose packing fraction $\eta_{rlp} \approx 0.59$. The critical value $\eta^* \approx 0.127$ is obtained in an excellent agreement with our numerical simulations.

For smaller particles, the transition between cluster and bouncing aggregate is also triggered when η increases. We have noted that the $\triangle$-frontier corresponds roughly to the relationship $r/L \sim \log N$ which consists in a Lambert-W function [29] provided by the inversion of (7).

$$\eta = \frac{4\pi}{3}\left(\frac{r}{L}\right)^3 \exp\frac{r_{ba} - r}{\delta_{ba}} \tag{7}$$

This transition curve needs deeper investigations since different bouncing modes (like period doubling) can be observed in some cases. This is left for future works.

The different values of the free fitting parameters for the various transition curves are given in table 1. In opposite to the small impact of the frequency, we can see that the variations are important when the amplitude changes.

A (mm)	f (Hz)	δ_{clust} (mm)	r_{clust} (mm)	δ_{ba} (mm)	r_{ba} (mm)
2.5	30	$6.8817\ 10^{-3}$	0.31908	$6.5718\ 10^{-2}$	0.75250
2.5	60	$6.3164\ 10^{-3}$	0.31239	$6.4548\ 10^{-2}$	0.74515
0.3	30	$9.2490\ 10^{-3}$	0.33101	-	-
0.3	60	$1.1143\ 10^{-2}$	0.34529	-	-

Table 1. Values of the free fitting parameters for the various transition curves in four diagrams

4.3. 3D Phase Diagram

In order to understand the origin of the cluster phenomenon, the internal energy of the system with amplitude $A = 2.5$ mm and $f = 30$ Hz has been investigated. By collecting the translation and the rotation velocities of the particles during one period, a three dimensional graph representing the mean kinematic energy in the system as a function of the packing fraction η and the grain radius r has been obtained. As shown in figure 9, the surface is colored by a color gradient and displays different energetic levels according to the dynamical regimes we determinate by statistical means. The corresponding transition lines shown in the previous figures are denoted by purple vertical surfaces.

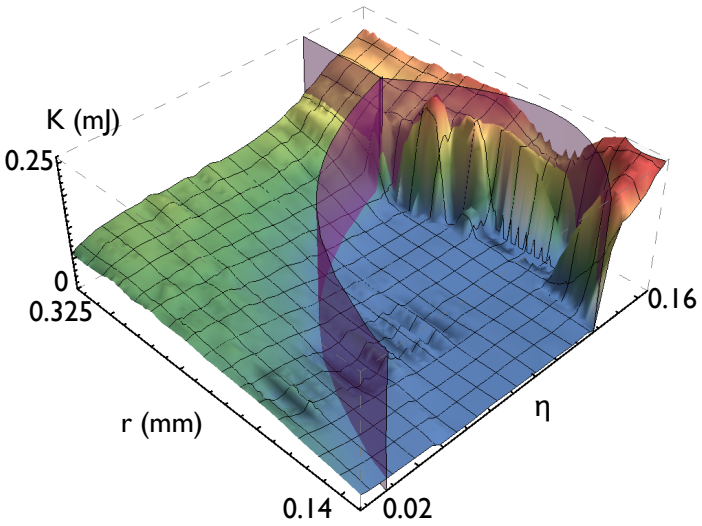

Figure 9. 3D view of the mean kinematic energy in the system with an amplitude $A = 2.5$ mm and frequency $f = 30$ Hz as a function of grain size r and packing fraction η. The corresponding transition lines shown in the previous figures are denoted by purple vertical surfaces.

5. Conclusion and Perspectives

In summary, the phase diagram is richer than expected since we have found four different dynamical regimes instead of gas/cluster regimes. Moreover, the transition curves cannot be described by simple rules or arguments, except for the behavior of large grains. Small variation of A and ω parameters will quantitatively modify the diagram but the phases and the transitions will be qualitatively recovered. We can assure that the diagram is locally stable. Our results raise fundamental questions and opens new perspectives in particular for future experiments in microgravity planned on the International Space Station.

In order to collect new relevant data, ESA is setting up "VIP-Gran", a series of experimentation expected to join the ISS in a closer future. In the experiment a certain amount of granular material is trapped in a cell volume of 30x30x70 mm between two independent oscillating walls. The main diagnostic tool is a CCD camera. Effects of the global packing fraction on the systems dynamics will be studied with a special interest in very dense systems and systems in a Knudsen regime. Different grain sizes as well as different shapes for the box will be tested. Moreover, experimentation with granular mixtures are planned. The following work has been realized in order to accomplish a first step for the calibration of VIP-Gran. Effects of parameters as grain size and packing fraction have been investigated and a granular phase diagram has been obtained.

6. Acknowledgments

We thank E. Falcon and S. Vincent-Bonnieu for fruitful discussions. This work has been supported by Prodex (Belspo, Brussels) and the European Space Agency program TT VIP-Gran. We also thank the TREX Morecar project (Feder, Wallonia) for supporting the development of our numerical model.

References

[1] O. Reynolds, Phil. Mag. Ser. **50**, 20 (1885)
[2] A. Kudrolli, Rep. Prog. Phys. **67**, 209 (2004)
[3] F. Ludewig and N. Vandewalle, Eur. Phys. J. E **18**, 367 (2005)
[4] D. Howell and R.P. Behringer, Phys. Rev. Lett. **82**, 5241 (1999)
[5] T.S. Majmudar and R.P. Behringer, Nature **435**, 1079 (2005)
[6] A. Kudrolli, M. Wollpert, J.P. Gollub, Phys. Rev. Lett. **78**, 1383 (1997)
[7] G. Lumay and N. Vandewalle, Phys. Rev. Lett. **95**, 028002 (2005)
[8] G. Lumay and N. Vandewalle, Phys. Rev. E. **74**, 021301 (2006)
[9] F. Ludewig, S. Dorbolo, T. Gilet and N. Vandewalle, Eur. Phys. Lett. **84**, 44001 (2008)
[10] P. A. Thomson and G. S. Grest, Phys. Rev. Lett. **67**, 13 (1991)
[11] G. D. R. Midi, Eur. Phys. J. E. **14**, 341(2004)
[12] P. deGennes, Rev. Mod. Phys. **71**, 374 (1999)
[13] A. M. Walsh, K. E. Holloway, P. Habdas and J. R. de Bruyn, Phys. Rev. Lett. **91**, 10 (2003)
[14] F. Spahn, J. Schmidt and M. Sremcevic, Lect. Notes in Phys. **557**, pp 507(2000)
[15] E. Falcon, R. Wunenburger, P. Evesque, S. Fauve, C. Chabot, Y. Garrabos and D. Beysens, Phys. Rev. Lett. **83**, 2, 440 (1999)
[16] E. Falcon, S. Fauve and C. Laroche, Eur. Phys. J. B **9**, 183 (1999)
[17] S. McNamara and W.R. Young, Phys. Rev. E. **50**, 1 (1994)
[18] P. Evesque, Y. Garrabos, C. Lecoutre, F. Palencia, and D. Beysens, Powders and Grains 2005 **1** (2005)
[19] S. McNamara and E. Falcon, Phys. Rev. E. **71**, 031302 (2005)
[20] S. Miller and S. Luding, Phys. Rev. E. **69**, 031305 (2004)
[21] P. A. Cundall and O. D. L. Stark, Geotechnique **29**, 47 (1979)
[22] F. Ludewig, PhD Thesis, University of Liege (2007)
(URL http://orbi.ulg.ac.be/handle/2268/70899)
[23] N. Taberlet, PhD Thesis, Université de Rennes I (2005)
[24] M. Hou, R. Liu, G. Zhai, Z. Sun, K. Lu, Y. Garrabos and P. Evesque, Microgravity Sci. Technol. **20**, 73 (2008)
[25] J. J. Brey and M. J. Ruiz-Montero, Phys. Rev. E. **67**, 021307 (2003)
[26] T. Gilet, N. Vandewalle and S. Dorbolo, Phys. Rev. E. **79**, 055201 (2009)
[27] W. T. Eadie, D. Drijard, F. E. James, M. Roos and B. Sadoulet, Statistical Methods in Experimental Physics, 2nd Edition (World Scientific, Amsterdam, 2006)
[28] N. Vandewalle, T. Gilet and S. Dorbolo (preprint 2010)
[29] S. R Valluri, D. J. Jeffrey and R. M. Corless, Canadian Journal of Physics **78**, 823 (2000)